

Spectral Line Survey toward a Molecular Cloud in IC10

Yuri Nishimura¹, Takashi Shimonishi^{2,3}, Yoshimasa Watanabe¹, Nami Sakai⁴,
Yuri Aikawa⁵, Akiko Kawamura⁶, and Satoshi Yamamoto¹

ABSTRACT

We have conducted a spectral line survey observation in the 3 mm band toward the low-metallicity dwarf galaxy IC10 with the 45 m radio telescope of Nobeyama Radio Observatory to explore its chemical composition at a molecular-cloud scale (~ 80 pc). The CS, SO, CCH, HCN, HCO⁺, and HNC lines are detected for the first time in this galaxy in addition to the CO and ¹³CO lines, while *c*-C₃H₂, CH₃OH, CN, C¹⁸O, and N₂H⁺ lines are not detected. The spectral intensity pattern is found to be similar to those observed toward molecular clouds in the Large Magellanic Cloud, whose metallicity is as low as IC10. Nitrogen-bearing species are deficient in comparison with the Galactic molecular clouds due to a lower elemental abundance of nitrogen. CCH is abundant in comparison with Galactic translucent clouds, whereas CH₃OH may be deficient. These characteristic trends for CCH and CH₃OH are also seen in the LMC, and seem to originate from photodissociation regions more extended in peripheries of molecular clouds due to the lower metallicity condition.

Subject headings: galaxies: individual (IC10) — galaxies: ISM — ISM: molecules

1. Introduction

The Local Group of galaxies comprises 50 or more galaxies, a majority of which are low-metallicity dwarf ones. Observations of such low-metallicity galaxies provide us with a clue to an understanding of chemical characteristics of distant galaxies in the early universe, which are in a metal-poor environment. It is generally thought that metallicity has a strong impact on chemical composition of molecular clouds (e.g., van Dishoeck & Black 1988; Millar & Herbst 1990). In a metal-poor environment, not only are metal-

bearing species less abundant, but production and destruction processes of molecules are expected to be different from those in a metal-rich environment. For example, photodissociation and photoionization are more effective in molecular clouds in low-metallicity conditions owing to the lower abundance of dust grains (e.g., Millar & Herbst 1990). Thus, detailed characterization of the chemical feature in low-metallicity galaxies is of fundamental importance in astrochemistry and astrophysics.

However, radio-astronomical observational studies on chemical composition of low-metallicity galaxies have so far been very sparse. Molecular line emission from low-metallicity galaxies is generally faint, and hence, observations have almost been limited to CO and its isotopologues. A notable exception is the Large Magellanic Cloud (LMC). Because of its proximity to the Sun ($d = 49.97 \pm 1.11$ kpc (Pietrzyński et al. 2013)), molecular line observations are carried out toward active star-forming regions (e.g., Chin et al. 1997; Heikkilä et al. 1999; Wang et al. 2009; Paron et al. 2014). Thanks to recent im-

¹Department of Physics, the University of Tokyo, 7-3-1, Hongo, Bunkyo-ku, Tokyo, 113-0033, Japan

²Frontier Research Institute for Interdisciplinary Sciences, Tohoku University, Aramaki-zaaoba 6-3, Aoba-ku, Sendai, Miyagi, 980-8578, Japan

³Astronomical Institute, Tohoku University, Aramaki-zaaoba 6-3, Aoba-ku, Sendai, Miyagi, 980-8578, Japan

⁴RIKEN, 2-1 Hirosawa, Wako, Saitama 351-0198, Japan

⁵Center for Computational Sciences, The University of Tsukuba, 1-1-1, Tennodai, Tsukuba, Ibaraki 305-8577, Japan

⁶National Astronomical Observatory of Japan, Osawa, Mitaka, Tokyo, 181-8588, Japan

provement of observing instruments, spectral lines of less abundant species are now observable in external galaxies with a reasonable observation time, which enable us to study their chemical compositions (e.g., Martín et al. 2006; Aladro et al. 2013; Watanabe et al. 2014). Such a situation is also true even for low-metallicity galaxies.

We recently conducted spectral line observations of molecular clouds in the LMC with the Mopra 22 m telescope as the initial step to characterize molecular-cloud-scale chemical composition characteristic to low-metallicity condition (Nishimura et al. 2016). We observed seven molecular clouds, which have different star-formation activities; two are quiescent molecular clouds which are not associated with infrared counterparts detected with *AKARI* or *Spitzer*, three are molecular clouds associated with high-mass star formation, and two are active star-forming clouds with the extended H II region. The difference of star-formation activities is reflected in infrared fluxes; their $8 \mu\text{m}$ fluxes vary from 26.8 to 946.8 mJy arcsec $^{-2}$ (38 arcsec beam averaged, *Spitzer*/IRAC, Meixner et al. 2006). We found that the chemical compositions of the 7 sources are similar to each other regardless of the large difference of star-formation activities. Since the beam size of the Mopra corresponds to the spatial resolution of 10 pc at the LMC distance, the major contribution to the observed spectra is rather diffuse molecular gas extending over the molecular clouds. The contribution from the star-forming cores seems to be smeared out in the observations. In other words, the observed chemical composition is characteristic to molecular clouds in the LMC.

By comparing the results with these observed in the metal-rich environment such as our Galaxy and the spiral arm of M51, the following two characteristics of the LMC spectra are found (Nishimura et al. 2016). (1) Nitrogen-bearing species (HCN, HNC, N_2H^+ , HNCO, CN) are obviously faint in the LMC, which originates from the low elemental abundance of nitrogen. (2) The lines of CCH are relatively brighter and the lines of CH_3OH are much weaker in the LMC than those in the spiral arm of M51. Moreover, the CCH/HCO $^+$ ratios in the LMC are higher than those found in the nearby translucent clouds in our Galaxy. This trend would originate from the stronger UV radiation field owing to the lower

abundance of dust grains.

We expect that these characteristics of the LMC can generally be found in other low-metallicity galaxies. To examine this prediction, we observed another low-metallicity galaxy IC10. IC10 is located at the distance of ~ 950 kpc (Hunter 2001), and its metallicity is lower by factor 5 than in Solar neighborhood (Garnett 1990). The star formation rate estimated from H α ($0.2M_\odot \text{ yr}^{-1}$; Gil de Paz et al. 2003) and the association of the large number of Wolf-Rayet stars (~ 100 ; Massey & Holmes 2002) imply active star formation in IC10. IC10 has been studied in C II ($158 \mu\text{m}$) (Madden et al. 1997), C I ($^3P_1 \rightarrow ^3P_0$) (Bolatto et al. 2000), and multi-transitions of CO (e.g., Petitpas & Wilson 1998; Bolatto et al. 2000; Leroy et al. 2006). However, molecular line observations except for CO and its isotopologues have not been reported.

2. Observations

The observations were carried out with the 45 m radio telescope at Nobeyama Radio Observatory (NRO) in February and March in 2015. We observed the most part of the frequency range from 84 to 116 GHz. We did not observe the frequency range of 91 – 91.5, 95.5 – 96, 100 – 103.5, and 107.5 – 108 GHz, because no spectral lines were detected in the LMC sources (Nishimura et al. 2016). The half-power beam width (HPBW) of the telescope is 20.4", 16.6" and 15.3" at 86, 110 and 115 GHz, respectively. They correspond to the spatial scale from 71.7 to 98.8 pc at the IC10 distance ($d = 950$ kpc). The telescope pointing was checked by observing a nearby SiO maser source (Y Cas) every hour, and the pointing accuracy was maintained to be better than 5". We observed two orthogonal polarization signals simultaneously by using the SIS mixer receiver (TZ1), whose system temperatures ranged from 120 to 280 K. The backend is the autocorrelator SAM45. The frequency resolution and bandwidth are 488.24 kHz and 1600 MHz, respectively. We binned 2 successive channels of SAM45 in the analysis to improve the signal-to-noise ratio. The resultant velocity resolution is 3.25 km s $^{-1}$ at 90 GHz. The line intensity was calibrated by the chopper wheel method, and a typical calibration accuracy is 20%. The antenna temper-

ature is divided by the main beam efficiency of 0.49 at 86 GHz, 0.42 at 100 GHz, and 0.40 at 115 GHz to obtain the main beam temperature T_{MB} . We employed the position-switching mode, where the on-source integration time of each scan was set to be 20 seconds for all the observations. The observed position is $\alpha_{\text{J2000}} = 00^{\text{h}}20^{\text{m}}27.9^{\text{s}}$, $\delta_{\text{J2000}} = 59^{\circ}17'01.0''$, where the ^{12}CO ($J = 1 - 0$) line intensity is the strongest in IC10 according to Leroy et al. (2006). The position is also confirmed to be bright in infrared (*JHK*, *Spitzer/IRAC* and *Spitzer/MIPS*, Lebouteiller et al. 2012). The off-source position is $3'$ away in azimuth from the on-source position. The total observation time was 55 hours (~ 18 hours for on-source). A typical rms noise temperature for each line in the T_{MB} scale is 2.5–8.0 mK for 84–112 GHz and 31–53 mK for 112–116 GHz at a frequency resolution of 976.5 kHz.

3. Results

Figure 1 shows the observed spectrum in the frequency range from 84 to 100 GHz, which is a part of the total observed spectrum. We detected the lines of CCH($N = 1 - 0$), HCN($J = 1 - 0$), HCO⁺($J = 1 - 0$), HNC($J = 1 - 0$; tentative detection), CS($J = 2 - 1$), and SO($N_J = 2_3 - 1_2$) in this frequency range for the first time. In addition, we also detected the lines of ^{13}CO ($J = 1 - 0$) and ^{12}CO ($J = 1 - 0$). On the other hand, the lines of *c*-C₃H₂($2_{12} - 1_{01}$), N₂H⁺($J = 1 - 0$), CH₃OH($J_k = 2_0 - 1_0$, A⁺), C¹⁸O($J = 1 - 0$), and CN($N = 1 - 0$) were not detected (Figure 2). Surprisingly, the spectral intensity pattern is very similar to that of the molecular cloud N44C in the LMC, although the molecular line intensities are weaker by a factor of about 1/6 than that toward N44C. Figure 3 (left) shows the integrated intensities of IC10 versus those of the LMC cloud N44C. Indeed a good correlation is seen between the two sources. The correlation coefficient is as high as 0.96. Even if the ^{13}CO data are excluded, it is 0.90. On the other hand, the spectrum toward IC10 significantly differs from that observed in the spiral arm of M51. This is also confirmed by the rather poor correlation in Figure 3 (right). The correlation coefficient is 0.83, while it is as low as 0.18 without ^{13}CO . As mentioned in Section 1, the spectrum of N44C reflects the GMC-scale chemical composition characteristic to the LMC, and

hence, the similarity seems to originate from the low-metallicity environment of IC10.

The line parameters derived by Gaussian fitting are summarized in Table 1. The velocity of the peak of the ^{12}CO line (-330.2 km s⁻¹) is consistent with the previous observation of the ^{12}CO ($J = 1 - 0$) line toward the same position with the Arizona Radio Observatory 12 m telescope (HPBW of $55''$) by Leroy et al. (2006) (-330.5 km s⁻¹). The integrated intensity of ^{12}CO observed by Leroy et al. (2006) is lower than ours only by a factor of 1.3, in spite of a large difference of the telescope beam size ($15.3''$ and $55.5''$). This result indicates that the ^{12}CO emitting region is at least extended over the beam size of the Nobeyama 45 m telescope. The v_{LSR} values of the detected lines range from -326 to -333 km s⁻¹, which are consistent with that of the ^{13}CO line. The line widths are mostly in the range from 12 km s⁻¹ to 16 km s⁻¹. Exceptions are the HNC line and one of the CCH lines (87.401989 GHz) probably due to a poor signal to noise ratio (3.8σ) and the blending of nearby hyperfine components, respectively (Figure 2).

We evaluated beam-averaged column densities by statistical equilibrium calculations, as we did for the LMC clouds (Nishimura et al. 2016). We employed the RADEX code (Van der Tak et al. 2007) for this purpose. Since only one rotational transition was observed for each molecular species, we assumed a range of the gas kinetic temperature to be from 10 K to 50 K, and a range of the H₂ density from 3×10^3 cm⁻³ to 1×10^6 cm⁻³. Although the H₂ density of 3×10^5 cm⁻³ and 10^6 cm⁻³ are seem too high for the H₂ density averaged over the 80 pc scale of molecular clouds, we assumed the wide range of the physical condition for robust estimate. The beam-averaged column densities are derived for the gas kinetic temperatures of 10 K, 20 K, 30 K, 40 K, and 50 K and the H₂ density of 3×10^3 cm⁻³, 1×10^4 cm⁻³, 3×10^4 cm⁻³, 1×10^5 cm⁻³, 3×10^5 cm⁻³, and 1×10^6 cm⁻³, as listed in Table 2.

4. Discussion

4.1. Effect of elemental abundances

Elemental abundances are different from galaxies to galaxies, reflecting the past history of star formation. In the low-metallicity galaxies, heavy

elements are generally deficient, and in particular, the deficiency of nitrogen is the most significant among the abundant second row elements (C, N, O) (Vincenzo et al. 2016). Because of this reason, one of the characteristic features in the chemical compositions would be the deficiency of the N-bearing molecules. The chemical model by Millar & Herbst (1990) indeed predicted that abundances of N-bearing species are sensitive to the elemental abundance of nitrogen. The deficiency of the N-bearing molecules is already evident in the spectral pattern of IC10 in comparison with that of the spiral arm of M51. We calculated the abundance ratios of HCN/HCO⁺ and HNC/HCO⁺ for IC10, under the assumption of the H₂ density of 3×10^3 , 1×10^4 , 3×10^4 , and 1×10^5 cm⁻³, 3×10^5 , and 1×10^6 cm⁻³, and the gas kinetic temperature of 10, 20, 30, 40, and 50 K, and compared them with the average ratios reported for the seven clouds in the LMC (Nishimura et al. 2016), the average ratios for three translucent clouds (CB17, CB24, CB228) in our Galaxy (Turner 1995b; Turner et al. 1997), and the ratio for the spiral arm position (P1) of M51 observed by Watanabe et al. (2014), as shown in Table 3. The observed spectrum of IC10 are averaged over molecular clouds (~ 80 pc scale), and seems to be dominated by the diffuse part of molecular clouds rather than dense star-forming cores. This is true even for smaller-scale observations (~ 10 pc scale) of the LMC clouds (Nishimura et al. 2016). Hence, for fair comparison, we chose the translucent clouds as representatives of our Galaxy. Although the column densities are sensitive to the assumed H₂ density and the assumed gas kinetic temperature, the column density ratios for IC10 are affected only less than $\pm 50\%$ in the parameter range. This fact is also shown in the analyses of the LMC spectra (Nishimura et al. 2016). The elemental N/O ratio in IC10 is lower by a factor of 3 than that in our Galaxy (Lequeux et al. 1979). The HCN/HCO⁺ and HNC/HCO⁺ ratios in IC10 are comparable to those for the LMC clouds, and are indeed found to be lower than in the three Galactic translucent clouds (CB17, CB24, CB228). Although the HCN/HCO⁺ ratios of IC10 and the Galactic translucent clouds marginally overlap with each other within the mutual error ranges, the overlap occurs only for the particular conditions that is not

very likely (3×10^3 cm⁻³ and 10 K for IC10 and 1×10^5 cm⁻³ and 50 K for the Galactic translucent clouds). Hence, we can state the above conclusion in spite of the formal error ranges. A similar comparison can also be made for M51 P1, which has the higher N/O ratio than the Solar neighborhood by a factor of 2 (Bresolin et al. 2004). The HCN/HCO⁺ and HNC/HCO⁺ ratios in M51 P1 are $8.4_{-4.6}^{+4.0}$ and $1.6_{-0.6}^{+0.6}$, respectively, which are higher than those in IC10 ($1.9_{-1.5}^{+1.9}$ and $0.4_{-0.2}^{+0.2}$, respectively). Hence, it is most likely that the deficiency of the N-bearing molecules directly reflects the elemental deficiency of nitrogen in the IC10.

The HCN/HCO⁺ ratio has been discussed for nuclear regions of external galaxies. The HCN/HCO⁺ ratio is known to be higher for the AGNs, which is interpreted as the effect of XDRs, cosmic-rays, and/or shock heatings (e.g., Lepp & Dalgarno 1996; Kohno et al. 2001; Meijerink et al. 2007; Aladro et al. 2015). In this study, we observed GMCs without such effects, and found the lower HCN/HCO⁺ ratio than the Galactic translucent clouds. Hence, the various effects suggested for the AGNs cannot be applied to IC10. Rather, the intrinsic effect of the elemental abundance can be seen in this source.

The CS/SO ratio in IC10 is $0.9_{-0.5}^{+0.5}$, which is comparable to that of the LMC ($1.8_{-0.3}^{+0.4}$). The ratio is also comparable to that in the Galactic translucent clouds ($1.0_{-0.5}^{+0.4}$), but is lower than that of M51 P1 ($4.6_{-1.8}^{+1.2}$). Any significant trend due to the difference of the C/O ratio is not seen in the CS/SO ratio in this study.

4.2. Effect of photodissociation

We calculated the abundance ratio of CCH/HCO⁺ in the same way as HCN/HCO⁺ and HNC/HCO⁺. The ratio of CCH/HCO⁺ is higher in IC10 ($20.9_{-9.2}^{+10.7}$) than in the Galactic translucent clouds ($5.3_{-2.4}^{+3.9}$) by a factor of 4. This enhancement of CCH in IC10 cannot be interpreted as the effect of elemental abundances. Indeed, the elemental C/O ratio is estimated to be 0.3 in IC10 (Lequeux et al. 1979; Bolatto et al. 2000), while it is 0.6 in Solar neighborhood. When the low C/O ratio is taken into account, the high CCH/HCO⁺ ratio in IC10 is striking. This enhancement of CCH is also seen in the LMC clouds (Nishimura et al. 2016).

The effect of photodissociation would be re-

sponsible for the enhancement. It is generally thought that CCH is abundant in the photodissociation region (PDR) illuminated by UV radiation (e.g., Pety et al. 2005; Martín et al. 2014; Ginard et al. 2015). In low-metallicity galaxies, the extinction of the UV radiation by dust grains is expected to be less effective for a given column density of H_2 because of the lower abundance of dust grains. The PDR would be extended deeper into molecular clouds, which would be responsible to the relatively high abundance of CCH. In the PDR, the growth of large carbon-chain molecules containing more than three carbon atoms are generally suppressed by competitive photodissociation processes (e.g., Lucas & Liszt 2000). The $c\text{-C}_3\text{H}_2/\text{CCH}$ ratio is indeed found to be less than 0.1 both in IC10 the LMC clouds, which is lower than that observed in the Galactic translucent clouds (0.22; Turner et al. 1999, 2000). The ratio is rather consistent with the ratio in some Galactic diffuse clouds observed in absorption against the bright continuum sources (0.04; Lucas & Liszt 2000) and the ratio in M82 which also hosts extended PDRs (0.04; Fuente et al. 2005; Aladro et al. 2015). This fact further supports the extended PDR in the low-metallicity galaxies.

Non-detection of CH_3OH is notable, as in the case of the LMC clouds (Nishimura et al. 2016). We obtained the upper limits of the CH_3OH intensity and the column density in IC10. The abundance ratio of $\text{CH}_3\text{OH}/\text{HCO}^+$ in IC10 is < 2.2 , which seems lower than that found in M51 ($3.8^{+5.8}_{-2.3}$). This result can also be interpreted in terms of a stronger UV effect owing to low abundance of dust grains in IC10. CH_3OH is thought to be produced by hydrogenation of CO on dust grains, and is liberated into the gas phase by thermal and/or non-thermal desorption (e.g., Watanabe & Kouchi 2002). A low abundance of dust grains tends to make the CH_3OH formation inefficient. Furthermore, laboratory experiments show that the efficiency of CH_3OH formation significantly decreases at the temperature higher than 20 K due to a fall of striking probability of hydrogen atom (Watanabe et al. 2003). Since the temperature of cloud peripheries is expected to be higher in the low-metallicity condition due to penetration of the UV radiation, CH_3OH would not be formed efficiently. Accord-

ing to Shimonishi et al. (2016), the lower abundance of CH_3OH ice observed in the LMC may be also caused by a relatively high dust temperature. Their result is consistent with ours.

We also evaluated the HNC/HCN ratio in IC10 to be $0.22^{+0.12}_{-0.11}$, which is comparable to the ratio in the LMC clouds, and is lower than the ratio in typical dark clouds (0.54 – 4.5; Hirota et al. 1998) in the Solar neighborhood. It is close to the ratio reported in some Galactic diffuse clouds, where the HCN and HNC lines are detected in absorption against bright continuum sources (0.21 ± 0.05 ; Liszt & Lucas 2001). Hirota et al. (1998) reported that the HNC/HCN ratio is lower under higher-temperature environments: the ratio decreases above 24 K, possibly reflecting isomerization mechanisms of HNC to HCN. The relatively low ratios observed in IC10 and the LMC clouds may also originate from warmer temperature conditions due to higher UV field and/or lower grain abundance. In addition, it is worth noting non-detection of N_2H^+ . This seems to originate mainly from the low elemental abundance of nitrogen. In addition, the UV radiation may also contribute to the low-abundance of N_2H^+ . Deeper penetration of UV radiation enhances the abundance of atomic ion and electrons, which efficiently destroys N_2H^+ (Aikawa et al. 2015).

5. Summary

The molecular-cloud-scale chemical composition of IC10 is found to be very similar to that of the LMC clouds. It is characterized by deficiency of N-bearing molecules, relatively high abundant CCH, and deficiency of CH_3OH . Hence, these chemical features can be regarded as ones characteristic in low-metallicity galaxies, although they have to be further examined in other galaxies with various metallicities. Furthermore, more sensitive observations are needed to detect larger molecules and explore the molecular evolution in low-metallicity galaxies.

We thank an anonymous reviewer for valuable comments. We thank the staff of the NRO 45 m telescope for excellent support. This study is partly supported from Grants-in-Aid of Education, Sports, Science, and Technologies of Japan (21224002, 25400223, and 25108005). YN is sup-

ported by Grant-in-Aid for JSPS Fellows (268280).

REFERENCES

- Aikawa, Y., Furuya, K., Nomura, H., & Qi, C. 2015, *ApJ*, 807, 120
- Aladro, R., Viti, S., Bayet, E., et al. 2013, *A&A*, 549, A39
- Aladro, R., Martín, S., Riquelme, D., et al. 2015, *A&A*, 579, A101
- Bolatto, A. D., Jackson, J. M., Wilson, C. D., & Moriarty-Schieven, G. 2000, *ApJ*, 532, 909
- Bresolin, F., Garnett, D. R., & Kennicutt, Jr., R. C. 2004, *ApJ*, 615, 228
- Chin, Y.-N., Henkel, C., Whiteoak, J. B., et al. 1997, *A&A*, 317, 548
- Dufour, R., Shields, G., & Talbot Jr, R. 1982, *ApJ*, 252, 461
- Fuente, A., García-Burillo, S., Gerin, M., et al. 2005, *ApJ*, 619, L155
- Garnett, D. R. 1990, *ApJ*, 363, 142
- Garnett, D. R., Edmunds, M. G., Henry, R. B. C., Pagel, B. E. J., & Skillman, E. D. 2004, *AJ*, 128, 2772
- Gil de Paz, A., Madore, B. F., & Pevunova, O. 2003, *ApJS*, 147, 29
- Ginard, D., Fuente, A., García-Burillo, S., et al. 2015, *A&A*, 578, A49
- Heikkilä, A., Johansson, L., & Olofsson, H. 1999, *A&A*, 344, 817
- Hirota, T., Yamamoto, S., Mikami, H., & Ohishi, M. 1998, *ApJ*, 503, 717
- Hunter, D. A. 2001, *ApJ*, 559, 225
- Kohno, K., Matsushita, S., Vila-Vilaró, B., et al. 2001, in *Astronomical Society of the Pacific Conference Series*, Vol. 249, *The Central Kiloparsec of Starbursts and AGN: The La Palma Connection*, ed. J. H. Knapen, J. E. Beckman, I. Shlosman, & T. J. Mahoney, 672
- Lebouteiller, V., Sloan, G., Groenewegen, M., et al. 2012, *A&A*, 546, A94
- Lepp, S., & Dalgarno, A. 1996, *A&A*, 306, L21
- Lequeux, J., Peimbert, M., Rayo, J., Serrano, A., & Torres-Peimbert, S. 1979, *A&A*, 80, 155
- Leroy, A., Bolatto, A., Walter, F., & Blitz, L. 2006, *ApJ*, 643, 825
- Liszt, H., & Lucas, R. 2001, *A&A*, 370, 576
- Lucas, R., & Liszt, H. 2000, *A&A*, 358, 1069
- Madden, S., Poglitsch, A., Geis, N., Stacey, G., & Townes, C. 1997, *ApJ*, 483, 200
- Magrini, L., & Gonçalves, D. R. 2009, *MNRAS*, 398, 280
- Martín, S., Mauersberger, R., Martín-Pintado, J., Henkel, C., & García-Burillo, S. 2006, *ApJS*, 164, 450
- Martín, S., Verdes-Montenegro, L., Aladro, R., et al. 2014, *A&A*, 563, L6
- Massey, P., & Holmes, S. 2002, *ApJ*, 580, L35
- Meijerink, R., Spaans, M., & Israel, F. P. 2007, *A&A*, 461, 793
- Meixner, M., Gordon, K. D., Indebetouw, R., et al. 2006, *The Astronomical Journal*, 132, 2268
- Millar, T. J., & Herbst, E. 1990, *MNRAS*, 242, 92
- Nishimura, Y., Shimonishi, T., Watanabe, Y., et al. 2016, *ApJ*, 818, 161
- . in prep.
- Paron, S., Ortega, M., Cunningham, M., et al. 2014, *A&A*, 572, A56
- Petitpas, G. R., & Wilson, C. D. 1998, *ApJ*, 496, 226
- Pety, J., Teyssier, D., Fossé, D., et al. 2005, *A&A*, 435, 885
- Pietrzyński, G., Graczyk, D., Gieren, W., et al. 2013, *Nature*, 495, 76
- Shimonishi, T., Dartois, E., Onaka, T., & Boulanger, F. 2016, *A&A*, 585, A107
- Turner, B. 1995a, *ApJ*, 455, 556

- . 1995b, *ApJ*, 449, 635
- . 1996, *ApJ*, 461, 246
- Turner, B., Herbst, E., & Terzieva, R. 2000, *ApJS*, 126, 427
- Turner, B., Pirogov, L., & Minh, Y. 1997, *ApJ*, 483, 235
- Turner, B., Terzieva, R., & Herbst, E. 1999, *ApJ*, 518, 699
- Van der Tak, F., Black, J. H., Schöier, F., Jansen, D., & van Dishoeck, E. F. 2007, *A&A*, 468, 627
- van Dishoeck, E. F., & Black, J. H. 1988, *ApJ*, 334, 771
- Vincenzo, F., Belfiore, F., Maiolino, R., Matteucci, F., & Ventura, P. 2016, *MNRAS*, 458, 3466
- Wang, M., Chin, Y.-N., Henkel, C., Whiteoak, J., & Cunningham, M. 2009, *ApJ*, 690, 580
- Watanabe, N., & Kouchi, A. 2002, *ApJ*, 571, L173
- Watanabe, N., Shiraki, T., & Kouchi, A. 2003, *ApJ*, 588, L121
- Watanabe, Y., Sakai, N., Sorai, K., & Yamamoto, S. 2014, *ApJ*, 788, 4

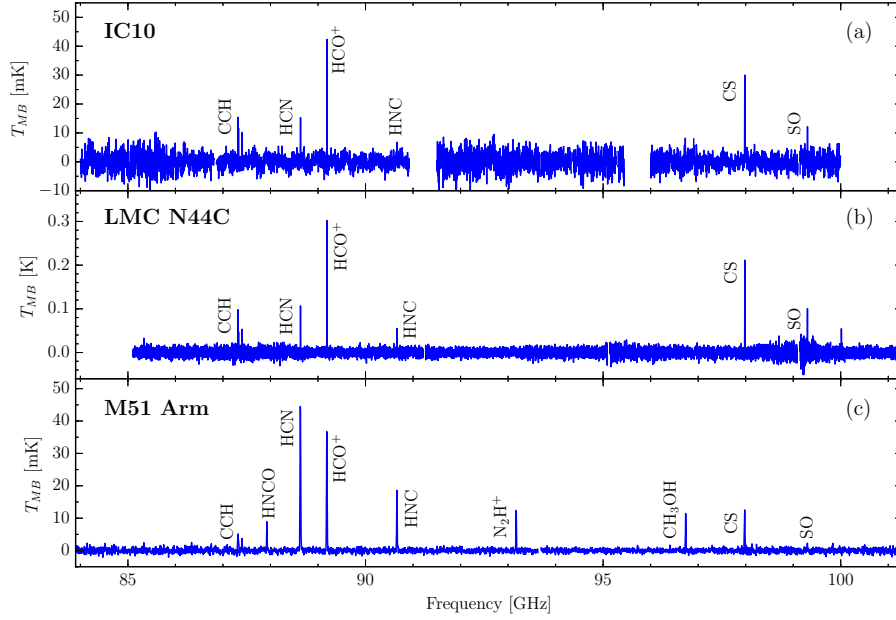


Fig. 1.— Compressed spectra observed toward (a) IC10, (b) LMC N44C (Nishimura et al. 2016), (c) the spiral arm of M51 (Watanabe et al. 2014). Note that the vertical scale is different from source to source.

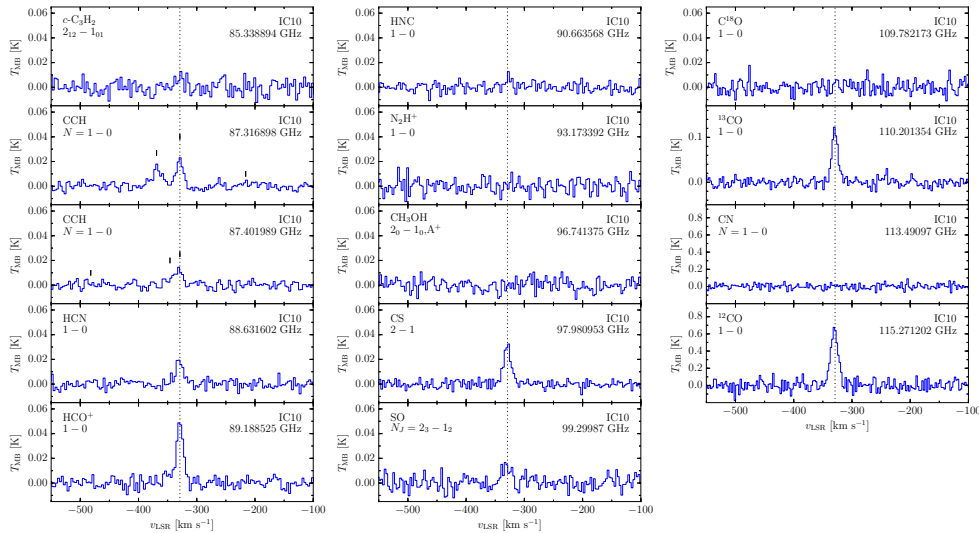


Fig. 2.— Spectral line profiles of individual molecular transitions observed in IC10. Small vertical lines in the CCH panel represent the positions of the hyperfine components.

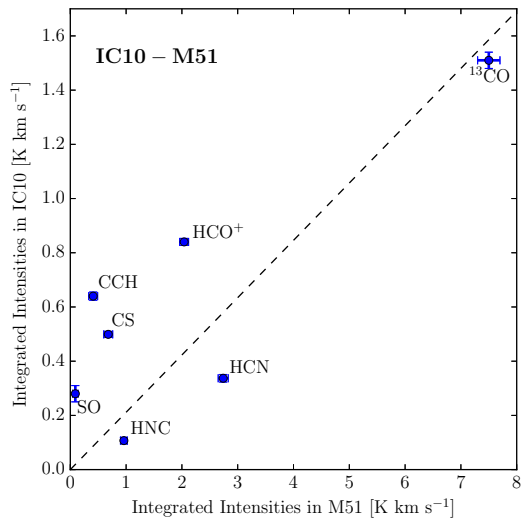
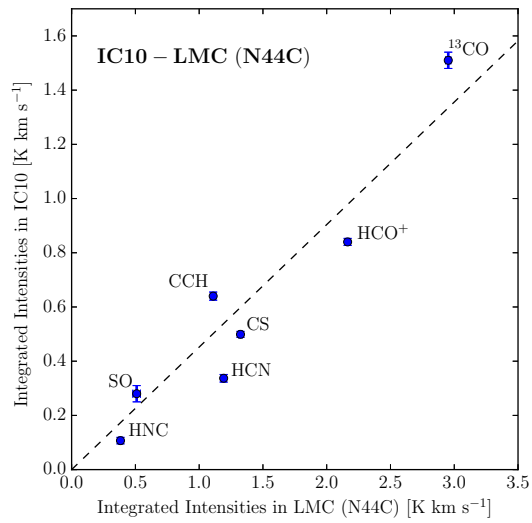


Fig. 3.— Correlation diagrams of integrated intensities of detected species between IC10 and LMC (N44C) (Nishimura et al. 2016) (*left*), and between IC10 and M51 (Watanabe et al. 2014) (*right*). The dashed line indicates the average ratio of the integrated intensities between the two sources.

TABLE 1
IC10 OBSERVED LINE PARAMETERS

Molecule	Frequency (GHz)	Transition	T_{MB} Peak (mK)	v_{LSR} (km s ⁻¹)	Δv (km s ⁻¹)	$\int T_{\text{MB}} dv$ (K km s ⁻¹)
<i>c</i> -C ₃ H ₂	85.338894	2 ₁₂ - 1 ₀₁				< 0.12
CCH	87.284105	$N = 1 - 0, J = 5/2 - 3/2, F = 1 - 1$				< 0.05
CCH	87.316898	$N = 1 - 0, J = 5/2 - 3/2, F = 2 - 1$	20 ± 2	-328.9 ± 0.6	15.5 ± 1.4	0.329 ± 0.015
CCH	87.328585	$N = 1 - 0, J = 5/2 - 3/2, F = 1 - 0$	15.7 ± 1.9	—	—	0.311 ± 0.014
CCH	87.401989	$N = 1 - 0, J = 3/2 - 3/2, F = 1 - 1$	12 ± 3	-333 ± 2	21 ± 5	0.28 ± 0.03
CCH	87.407165	$N = 1 - 0, J = 3/2 - 3/2, F = 0 - 1$	—	—	—	—
CCH	87.446470	$N = 1 - 0, J = 3/2 - 3/2, F = 1 - 0$				< 0.05
HCN	88.631602	1 - 0	19 ± 2	-329.8 ± 0.8	15 ± 2	0.337 ± 0.014
HCO ⁺	89.188525	1 - 0	49 ± 2	-328.9 ± 0.3	13.9 ± 0.8	0.840 ± 0.013
HNC	90.663568	1 - 0	10 ± 3	-326.7 ± 1.2	9 ± 3	0.107 ± 0.012
N ₂ H ⁺	93.173392	1 - 0				< 0.11
CH ₃ OH	96.741375	2 ₀ - 1 ₀ , A ⁺				< 0.09
CS	97.980953	2 - 1	30.7 ± 1.6	-329.2 ± 0.4	15.0 ± 0.9	0.499 ± 0.011
SO	99.299870	$N_J = 2_3 - 1_2$	14 ± 3	-331.2 ± 1.7	18 ± 4	0.28 ± 0.03
C ¹⁸ O	109.782173	1 - 0				< 0.10
¹³ CO	110.201354	1 - 0	118 ± 5	-329.4 ± 0.3	12.0 ± 0.6	1.51 ± 0.03
CN	113.490970	$N = 1 - 0, J = 3/2 - 1/2, F = 5/2 - 3/2$				< 0.6
¹² CO	115.271202	1 - 0	653 ± 31	-330.2 ± 0.3	15.1 ± 0.8	10.4 ± 0.2

NOTE.—The errors are 1 σ . The upper limits are 3 σ . The calibration error ($\sim 20\%$) is not included.

TABLE 2
DERIVED COLUMN DENSITIES^a

molecule	n_{H_2}	$3 \times 10^3 \text{ cm}^{-3}$				
	T_k	10 K	20 K	30 K	40 K	50 K
<i>c</i> -C ₃ H ₂ (ortho)	< 2.7(+13)	< 1.1(+13)	< 6.7(+12)	< 5.5(+12)	< 5.2(+12)	
CCH	2.4(+14)	1.1(+14)	8.6(+13)	7.1(+13)	6.2(+13)	
HCN	5.3(+13)	2.8(+13)	2.2(+13)	1.9(+13)	1.6(+13)	
HCO ⁺	1.4(+13)	8.3(+12)	6.7(+12)	5.8(+12)	5.3(+12)	
HNC	6.1(+12)	4.1(+12)	3.6(+12)	3.3(+12)	3.1(+12)	
N ₂ H ⁺	< 1.8(+12)	< 1.1(+12)	< 9.2(+11)	< 8.0(+11)	< 7.3(+11)	
CH ₃ OH (A)	< 8.7(+12)	< 4.9(+12)	< 4.0(+12)	< 3.6(+12)	< 3.4(+12)	
CS	6.5(+13)	3.8(+13)	3.0(+13)	2.5(+13)	2.3(+13)	
SO	6.0(+13)	2.8(+13)	2.1(+13)	1.8(+13)	1.6(+13)	
C ¹⁸ O	< 8.5(+13)	< 7.8(+13)	< 8.1(+13)	< 8.5(+13)	< 8.9(+13)	
¹³ CO	1.3(+15)	1.2(+15)	1.2(+15)	1.3(+15)	1.3(+15)	
CN	< 5.0(+14)	< 2.2(+14)	< 1.5(+14)	< 1.1(+14)	< 9.4(+13)	
¹² CO	9.2(+15)	7.8(+15)	7.9(+15)	8.2(+15)	8.6(+15)	

molecule	n_{H_2}	$1 \times 10^4 \text{ cm}^{-3}$				
	T_k	10 K	20 K	30 K	40 K	50 K
<i>c</i> -C ₃ H ₂ (ortho)	< 7.9(+12)	< 3.3(+12)	< 2.1(+12)	< 1.8(+12)	< 1.7(+12)	
CCH	7.8(+13)	4.1(+13)	3.2(+13)	2.8(+13)	2.5(+13)	
HCN	1.4(+13)	8.2(+12)	6.4(+12)	5.5(+12)	4.9(+12)	
HCO ⁺	4.3(+12)	2.7(+12)	2.2(+12)	1.9(+12)	1.8(+12)	
HNC	1.8(+12)	1.3(+12)	1.1(+12)	1.0(+12)	9.9(+11)	
N ₂ H ⁺	< 6.0(+11)	< 3.8(+11)	< 3.2(+11)	< 2.8(+11)	< 2.6(+11)	
CH ₃ OH (A)	< 3.5(+12)	< 2.3(+12)	< 2.0(+12)	< 1.9(+12)	< 1.8(+12)	
CS	2.0(+13)	1.2(+13)	9.5(+12)	8.2(+12)	7.4(+12)	
SO	1.9(+13)	9.4(+12)	7.2(+12)	6.3(+12)	5.7(+12)	
C ¹⁸ O	< 8.6(+13)	< 9.6(+13)	< 1.1(+14)	< 1.3(+14)	< 1.4(+14)	
¹³ CO	1.3(+15)	1.5(+15)	1.7(+15)	1.9(+15)	2.1(+15)	
CN	< 1.3(+14)	< 6.0(+13)	< 4.2(+13)	< 3.4(+13)	< 2.9(+13)	
¹² CO	8.9(+15)	9.4(+15)	1.1(+16)	1.2(+16)	1.3(+16)	

molecule	n_{H_2}	$3 \times 10^4 \text{ cm}^{-3}$				
	T_k	10 K	20 K	30 K	40 K	50 K
<i>c</i> -C ₃ H ₂ (ortho)	< 2.8(+12)	< 1.3(+12)	< 8.7(+11)	< 7.6(+11)	< 7.3(+11)	
CCH	3.4(+13)	2.1(+13)	1.8(+13)	1.6(+13)	1.6(+13)	
HCN	4.9(+12)	2.8(+12)	2.3(+12)	2.0(+12)	1.8(+12)	
HCO ⁺	1.7(+12)	1.2(+12)	1.0(+12)	9.3(+11)	8.8(+11)	
HNC	6.9(+11)	4.9(+11)	4.3(+11)	4.1(+11)	3.9(+11)	
N ₂ H ⁺	< 2.6(+11)	< 1.8(+11)	< 1.5(+11)	< 1.4(+11)	< 1.4(+11)	
CH ₃ OH (A)	< 2.2(+12)	< 1.7(+12)	< 1.7(+12)	< 1.7(+12)	< 1.8(+12)	
CS	7.5(+12)	4.7(+12)	3.9(+12)	3.5(+12)	3.2(+12)	
SO	7.4(+12)	4.2(+12)	3.5(+12)	3.2(+12)	3.1(+12)	
C ¹⁸ O	< 9.3(+13)	< 1.2(+14)	< 1.4(+14)	< 1.7(+14)	< 1.9(+14)	
¹³ CO	1.4(+15)	1.7(+15)	2.1(+15)	2.5(+15)	2.9(+15)	
CN	< 4.1(+13)	< 2.1(+13)	< 1.5(+13)	< 1.3(+13)	< 1.1(+13)	
¹² CO	9.5(+15)	1.1(+16)	1.4(+16)	1.6(+16)	1.8(+16)	

TABLE 2—Continued

molecule	n_{H_2}	$1 \times 10^5 \text{ cm}^{-3}$				
	T_k	10 K	20 K	30 K	40 K	50 K
<i>c</i> -C ₃ H ₂ (ortho)		< 1.0(+12)	< 5.6(+11)	< 4.7(+11)	< 4.5(+11)	< 4.4(+11)
CCH		1.9(+13)	1.5(+13)	1.5(+13)	1.5(+13)	1.6(+13)
HCN		1.7(+12)	1.0(+12)	8.7(+11)	7.8(+11)	7.2(+11)
HCO ⁺		8.9(+11)	6.9(+11)	6.5(+11)	6.3(+11)	6.3(+11)
HNC		2.9(+11)	2.2(+11)	2.0(+11)	1.9(+11)	1.8(+11)
N ₂ H ⁺		< 1.4(+11)	< 1.1(+11)	< 1.0(+11)	< 1.0(+11)	< 1.0(+11)
CH ₃ OH (A)		< 1.9(+12)	< 1.9(+12)	< 2.1(+12)	< 2.3(+12)	< 2.5(+12)
CS		3.3(+12)	2.3(+12)	2.1(+12)	2.0(+12)	1.9(+12)
SO		3.8(+12)	2.8(+12)	2.7(+12)	2.7(+12)	2.8(+12)
C ¹⁸ O		< 9.7(+13)	< 1.3(+14)	< 1.6(+14)	< 2.0(+14)	< 2.3(+14)
¹³ CO		1.5(+15)	1.9(+15)	2.5(+15)	3.0(+15)	3.5(+15)
CN		< 1.4(+13)	< 7.9(+12)	< 6.2(+12)	< 5.4(+12)	< 4.9(+12)
¹² CO		9.9(+15)	1.2(+16)	1.6(+16)	1.9(+16)	2.2(+16)

molecule	n_{H_2}	$3 \times 10^5 \text{ cm}^{-3}$				
	T_k	10 K	20 K	30 K	40 K	50 K
<i>c</i> -C ₃ H ₂ (ortho)		< 5.5(+11)	< 4.3(+11)	< 4.8(+11)	< 5.2(+11)	< 5.4(+11)
CCH		1.7(+13)	1.7(+13)	1.9(+13)	2.1(+13)	2.4(+13)
HCN		7.8(+11)	5.5(+11)	4.9(+11)	4.6(+11)	4.4(+11)
HCO ⁺		7.1(+11)	6.6(+11)	6.8(+11)	7.2(+11)	7.5(+11)
HNC		1.8(+11)	1.5(+11)	1.4(+11)	1.4(+11)	1.3(+11)
N ₂ H ⁺		< 1.2(+11)	< 1.1(+11)	< 1.1(+11)	< 1.2(+11)	< 1.3(+11)
CH ₃ OH (A)		< 2.0(+12)	< 2.2(+12)	< 2.7(+12)	< 3.1(+12)	< 3.5(+12)
CS		2.2(+12)	1.8(+12)	1.8(+12)	1.9(+12)	1.9(+12)
SO		3.1(+12)	3.0(+12)	3.4(+12)	3.8(+12)	4.1(+12)
C ¹⁸ O		< 9.8(+13)	< 1.3(+14)	< 1.7(+14)	< 2.1(+14)	< 2.6(+14)
¹³ CO		1.5(+15)	2.0(+15)	2.6(+15)	3.2(+15)	3.9(+15)
CN		< 6.6(+12)	< 4.4(+12)	< 3.8(+12)	< 3.6(+12)	< 3.6(+12)
¹² CO		1.0(+16)	1.3(+16)	1.7(+16)	2.0(+16)	2.4(+16)

molecule	n_{H_2}	$1 \times 10^6 \text{ cm}^{-3}$				
	T_k	10 K	20 K	30 K	40 K	50 K
<i>c</i> -C ₃ H ₂ (ortho)		< 4.5(+11)	< 5.8(+11)	< 8.7(+11)	< 1.1(+12)	< 1.2(+12)
CCH		1.8(+13)	2.3(+13)	2.8(+13)	3.3(+13)	3.8(+13)
HCN		5.0(+11)	4.3(+11)	4.3(+11)	4.4(+11)	4.5(+11)
HCO ⁺		7.4(+11)	8.5(+11)	1.0(+12)	1.1(+12)	1.3(+12)
HNC		1.5(+11)	1.4(+11)	1.4(+11)	1.5(+11)	1.5(+11)
N ₂ H ⁺		< 1.2(+11)	< 1.4(+11)	< 1.7(+11)	< 2.0(+11)	< 2.2(+11)
CH ₃ OH (A)		< 2.1(+12)	< 2.6(+12)	< 3.3(+12)	< 4.0(+12)	< 4.7(+12)
CS		2.1(+12)	2.1(+12)	2.3(+12)	2.6(+12)	2.9(+12)
SO		3.2(+12)	3.8(+12)	4.8(+12)	5.7(+12)	6.5(+12)
C ¹⁸ O		< 9.9(+13)	< 1.3(+14)	< 1.8(+14)	< 2.2(+14)	< 2.7(+14)
¹³ CO		1.5(+15)	2.0(+15)	2.7(+15)	3.4(+15)	4.0(+15)
CN		< 4.2(+12)	< 3.6(+12)	< 3.7(+12)	< 3.9(+12)	< 4.2(+12)
¹² CO		1.0(+16)	1.3(+16)	1.7(+16)	2.1(+16)	2.5(+16)

^a $a(+b)$ refers to $a \times 10^{+b} \text{ cm}^{-2}$.

TABLE 3
COLUMN DENSITY AND ELEMENTAL ABUNDANCE RATIOS.

		IC10	LMC	“Solar”	M51
Elemental abundance ratio	N/O	0.04	0.036	0.12	~ 0.25
	C/O	0.3	0.33	0.60	~ 0.6
	S/O	~ 0.03	0.043	0.023	~ 0.025
Column density ratio	$N[\text{HCN}]/N[\text{HCO}^+]$	$1.9^{+1.9}_{-1.5}$	$4.0^{+0.6}_{-1.0}$	$8.0^{+2.9}_{-4.6}$	$8.4^{+4.0}_{-4.6}$
	$N[\text{HNC}]/N[\text{HCO}^+]$	$0.4^{+0.2}_{-0.2}$	$0.85^{+0.15}_{-0.12}$	$3.4^{+1.3}_{-1.2}$	$1.6^{+0.6}_{-0.6}$
	$N[\text{HNC}]/N[\text{HCN}]$	$0.22^{+0.12}_{-0.11}$	$0.23^{+0.06}_{-0.06}$	$0.4^{+0.2}_{-0.2}$	$0.21^{+0.07}_{-0.07}$
	$N[\text{CCH}]/N[\text{HCO}^+]$	$20.9^{+10.7}_{-9.2}$	$12.4^{+3.3}_{-3.1}$	$5.3^{+3.9}_{-2.4}$	$9.1^{+3.8}_{-2.9}$
	$N[\text{CS}]/N[\text{HCO}^+]$	$3.5^{+1.1}_{-1.3}$	$4.6^{+0.3}_{-0.5}$	$3.4^{+0.5}_{-0.7}$	$2.3^{+0.4}_{-0.6}$
	$N[\text{CS}]/N[\text{SO}]$	$0.9^{+0.3}_{-0.5}$	$1.8^{+0.4}_{-0.3}$	$1.0^{+0.4}_{-0.5}$	$4.6^{+1.2}_{-1.8}$

NOTE.—Elemental abundances are based on Lequeux et al. (1979); Bolatto et al. (2000); Magrini & Gonçalves (2009) for IC10, Dufour et al. (1982) for the LMC and “Solar”, Bresolin et al. (2004); Garnett et al. (2004) for M51. Column densities of the LMC are calculated for the H_2 density range of $3 \times 10^3 - 3 \times 10^4 \text{ cm}^{-3}$ and the gas kinetic temperature range of 10 – 30 K, based on the literature data (Nishimura et al. 2016). Those for “Solar” (nearby translucent clouds; CB17, CB24, CB228) (Turner 1995a,b, 1996; Turner et al. 1997, 2000) are calculated for the H_2 density range of $3 \times 10^3 - 1 \times 10^5 \text{ cm}^{-3}$ and the gas kinetic temperature range of 10 – 50 K. We choose these clouds, because all molecules listed in this table are observed. For M51, we calculated the column densities under the assumption of H_2 density of $3 \times 10^3 - 1 \times 10^5 \text{ cm}^{-3}$ and the gas kinetic temperature of 10 – 50 K, based on the literature data (Watanabe et al. 2014). Note that the H_2 density is derived toward this source to be $\sim 10^4 \text{ cm}^{-3}$ by observations of the H_2CO lines (Nishimura et al. in prep.). The errors are estimated from the variation due to the assumed gas kinetic temperature and H_2 density.